等离子—MIG 焊接起弧过程

李德元，　张义顺，　董晓强
（沈阳工业大学 材料科学与工程学院，沈阳　110023）

摘　要：采用 Paschen 定律对电弧空间内不同起弧路径上的击穿电压进行了计算，分析等离子—MIG 双电弧焊接时的起弧过程，研究了击穿长度和温度对起弧过程的共同作用；成功地解释了等离子电弧借助 MIG 电弧提供的导电通道引燃的过程。结果表明，在分析电弧空间各不同路径上最小击穿电压时，除了要考虑击穿间隙的大小外，还必须考虑到温度的分布和保护气氛的种类。Paschen 定律可以对这几个因素的共同影响进行分析，从而有效地预测了后引燃电弧的起弧路径，这种方法也可以推广到其它双电弧焊接方法。通过高速摄像拍摄，对实际的起弧过程进行了分析，验证了计算的结果。

关键词：焊接；等离子弧；MIG 电弧；起弧；Paschen 定律
中图分类号：TG403　　文献标识码：A　　文章编号：0253－360X(2007)11－089－04

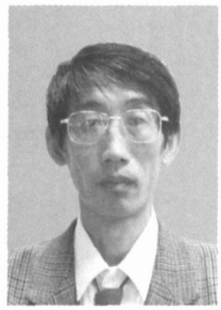

李德元

0　序　　言

等离子—MIG 焊接是一种采用复合双电弧完成焊接的高效焊接方法，充分利用了等离子弧能量密度高、电弧刚度好的特点和 MIG 电弧焊接效率高、提供填充金属能力强的特点，可以实现高效率焊接[1]。目前这种方法主要被用于有色金属的焊接，特别是在铝和铝合金的焊接方面，更有其它焊接方法难以比拟的优点[2]。

由于等离子—MIG 焊接是一种靠双电弧来完成焊接的方法，其电弧的形态往往要比一般的单电弧焊接时更复杂。当焊接铝及铝合金时，由于通常是采用环形铜电极作为阳极，等离子电弧的阳极斑点可以在阳极上不同的位置产生，使双电弧的组态可以出现多种复杂的情况。这些不同的电弧组态对焊接的效果会产生很大的影响。但在国内外关于这种焊接方法的研究文献中，对其电弧形态方面的研究还很少。Ton 等人[3] 曾分析了等离子—MIG 焊接电弧的物理特性，认为等离子—MIG 电弧是一种外廓温度高，中心温度反而比较低的分层电弧；Essers 等人[4] 曾研究了等离子—MIG 焊接电弧中的熔滴过渡特征。但这些研究都没有涉及到双电弧的起弧过程，也没有涉及到两个电弧之间相互作用的问题。为了对等离子—MIG 双电弧的起弧过程及焊接特性进行更深入的分析，利用有限元方法分析了电弧空间的流动和温度分布情况，利用气体击穿的相关理论与实际观察相比较，分析了双电弧的起弧过程及其对复合电弧形态的影响。

1　电弧空间流场和温度场的模拟

在等离子—MIG 焊接方法中，MIG 电弧是在位于枪体中心的焊丝与工件之间产生，总是位于电弧的中心位置；而等离子电弧则通常是在围绕着焊丝的环形喷嘴上产生。计算模型所设定的情况是 MIG 电弧已经引燃并稳定燃烧，且电弧附近的气体已经被该电弧充分加热，形成了准稳定温度场的情况。计算中所采用的简化物理模型如图 1 所示。焊丝材料为纯铝，枪体其它部分为纯铜，工件的尺寸设为无穷大，材料为纯铝。流动分析时的边界条件如下：气体种类为氩气，其流动方向如图中粗实线箭头所示；设定氩气入口流速为0.3 m/s。温度分析的边界条件如下：所计算的是存在气体流动和换热条件下的

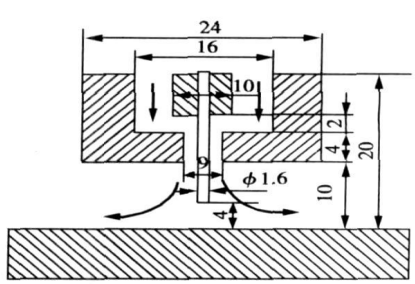

图 1　计算简化模型(mm)
Fig. 1　Simplified calculation model

收稿日期：2007－05－18

温度场。枪体和工件的初始温度为25 ℃;表面的自然对流系数为3.42 W/(m^2·K);MIG 电弧的温度为8 000 ℃;MIG 电弧的热流密度为36.45 MW/m^2,热源功率为3 276 W。纯铝的熔化潜热 $L=3.894\times10^5$ J/kg;铝的熔点为660 ℃。利用 ANSYS 软件计算得到的电弧空间的流场和温度场分布如图 2 所示。

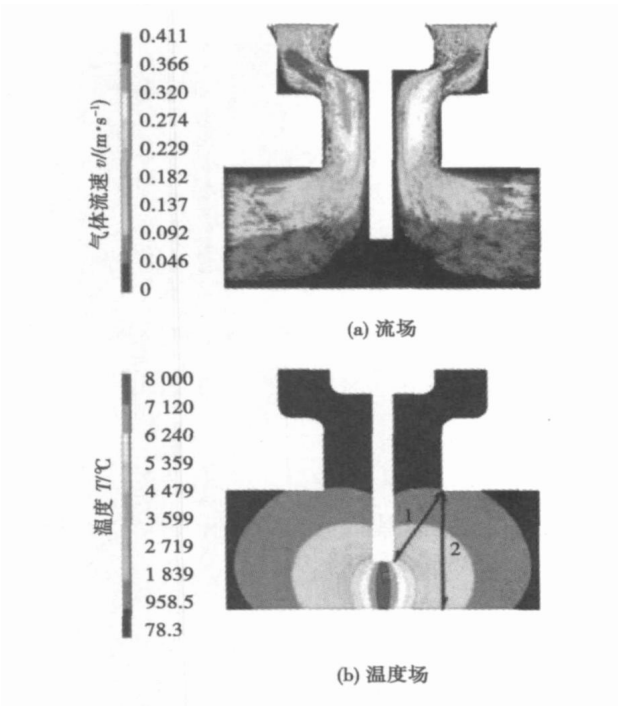

图 2 电弧空间的流场和温度场

Fig. 2 Flow field and temperature field around arc

2 Paschen 自变量设定及其应用

2.1 关于 Paschen 自变量的设定

式(1)为 Paschen 定律,这是有关气体击穿的一个重要定律,在研究高电压绝缘等领域中获得广泛应用[5]。

$$U_s=\frac{Bpd}{\ln\left[\frac{Apd}{\ln(1+1/\gamma)}\right]},\qquad(1)$$

式中:U_s 为气体击穿电压;d 为两极间的距离;p 为气体压力;A, B 均为试验常数;γ 为二次电子发射系数。

根据 Paschen 定律,气体的击穿电压不纯是气压 p 和极间间距 d 的函数,而且是 p 与 d 乘积的函数。

电弧气氛中的气体为氩气,根据由 Petre 等人[6]在采用简单阴极情况下所得到的氩气的击穿电位曲线进行线性回归,可以得到适用于氩气的击穿公式,即

$$U_s=0.24pd+0.17。\qquad(2)$$

以上的分析是在假定气体温度不变的情况下得到的。考虑温度变化的影响,采用 Paschen 定律的另一种更普遍的形式,以气体的密度 δ 代替压力,对空气来说,可表示为如下的经验公式[7],即

$$U_s=24.55\,\delta d+6.66\sqrt{\delta d}。\qquad(3)$$

对于氩气来说,还没有类似的经验公式,但根据其 Paschen 曲线的形状,同样可以推论出以下的结论:即其击穿电压 $U_s=f(\delta d)=F(pd/T)$,此函数在 Paschen 曲线最小值右侧的范围内应该为一个增函数,即随着 pd/T 的增大,击穿电压的值也将增大。根据这种分析,在研究 U_s 相对大小时,只要分析函数中的自变量 pd/T 的相对大小就可以了。在所研究的范围内,pd/T 越小,则对应的 U_s 也将越小。

当需要对不同部位的击穿电压进行比较时,直接采用比较 Paschen 自变量 pd/T 的方法,通过比较该自变量,来确定各不同击穿路径上的击穿电压。

需要特殊解释的是 Paschen 定律的适用范围是有限的,一般仅适用于自持放电阶段,而焊接电弧属于弧光放电状态,当电弧一旦引燃,它的电压将迅速下降,从几百伏迅速降低到几十伏、甚至几伏的数量级。此时,电弧中的气体已经高度电离,因此不符合 Paschen 定律的适用范围。

一个特殊的情况在于有两个电弧存在。MIG 电弧首先引燃,而等离子电弧的起弧过程是在电弧空间已经被 MIG 电弧加热后才发生,相当于讨论在加热气体中击穿的问题,这却属于 Paschen 定律可以应用的情况。用 Paschen 定律进行分析时,把先引燃的电弧作为一个加热气体的热源来考虑,然后分析第二个电弧的击穿和引燃过程。

2.2 平坦环形阳极上的起弧过程分析

这里讨论的是在平坦环形铜阳极上随机起弧的情况。如图 1 所示。当 MIG 电弧首先引燃后,电弧空间的气体被加热。由于枪体喷嘴与工件之间存在一个由等离子电源提供的约80 V的空载电压,如果能达到氩气击穿的条件,等离子电弧就会被引燃。研究中首先采用有限元方法对温度场进行了分析,所得到的电弧区的温度分布情况如图 2b 所示。在计算过程中,首先利用 ANSYS 温度计算的结果,对所分析的起弧路径上的温度进行选线分析,绘制出该路径上的温度分布图,然后进行积分求和,并计算平均温度 T。根据对 d 和 T 的综合分析,该空间内最有可能击穿的位置有两个,分别是位于环形电极的内缘与焊丝之间(路径 1),此路径上击穿距离最小,平均温度 T 最高,但电位差相对比较小。另一个则是处于喷嘴内缘与工件之间(路径 2),此处温度也比较高,击穿距离大一些,但电位差比较大。

根据计算分析，在路径 1 上的平均温度为 3 195.5 K，在路径 2 上的平均温度为2 087.7 K。带入Paschen 自变量 $x=pd/T$，并假定 p 为常量。则在路径 1 上 $x=2.35\times10^{-3}p$；而在路径 2 上，$x=4.79\times10^{-3}p$。显然路径 1 上具有更好的击穿条件。但是在算例中有一个需要特殊考虑的问题，就是作用在路径 2 上的电压为 $U_2=U_{\text{plasma空载}}\approx80$ V，而作用于路径1 上的电压为 $U_1=U_{\text{plasma空载}}-U_{\text{MIG}}\approx80$ V－22 V＝58 V。引入等效场强 $E_i=U_i/x_i$ 进行修正，得到在路径 1 上，$E_1=24.68\times10^3/p$；而在路径 2 上，$E_2=16.70\times10^3/p$；$E_1>E_2$；表明路径 1 上仍具有更好的击穿条件，所以在这种情况下，等离子电弧仍将沿着路径 1 引燃，也就是说在如图 1布置的情况下，等离子电弧将借助于MIG 电弧形成的导电通路引燃。

2.3　阳极上带有导弧点的情况

如前面所分析的情况，采用平坦环电极时引弧并不困难，但由于环形电极内缘各处与焊丝之间的导通条件都是相同的，当热量波动时，阳极斑点将在阳极上发生跳动，这会导致焊接过程的不稳定。解决的方法之一是在环形电极上设置凸起的导弧点，保持电弧弧根的稳定。考虑到喷嘴后部位于熔池上方容易与焊缝余高部分接触，同时还容易受到焊接飞溅的污染，因此将导弧点设计在喷嘴的前部，导弧点横向的中心对准焊缝中心线。如图 3 所示，是在喷嘴内缘处设置高度为4 mm的导弧点后，电弧空间的温度分布情况。

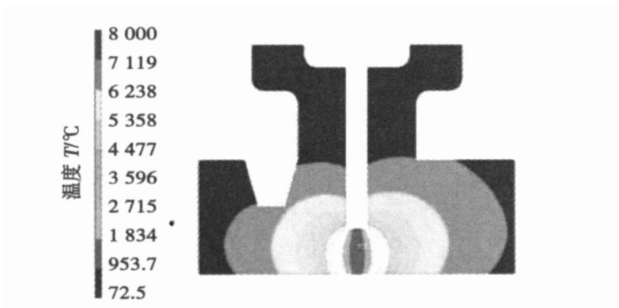

图 3　导弧点长度为 4 mm 时的温度分布

Fig. 3　Temperature distribution with a 4mm leading arc point length

由图中可见，设置导弧点后，气体击穿间隙 d 将明显变小，但导弧点又远离了电弧空间的高温区，会使击穿路径上的温度 T 下降。通过计算表明，当导弧点长度分别为 2，4 和6 mm时，在导弧点与工件之间的间隙内，平均温度将分别为1 716.4，1 729.2 和1 674.3 K；此时它们所对应的 Paschen 自变量 pd/T分别为 $4.66\times10^{-3}p$，$3.47\times10^{-3}p$ 和 $2.39\times10^{-3}p$。与图 2b 中给出的由喷嘴到焊丝起弧路径 1 上的等效场强$24.68\times10^3/p$相比，导弧点为4 mm时的等效场强为$23.05\times10^3/p$，仍然略小于路径 1 上的等效场强，说明此时导弧点并不能保证有效引燃。而当其长度为6 mm时，等效场强为$33.47\times10^3/p$，已经优于路径 1 的起弧条件，此时导弧点可以有效地保证导弧的成功。但由于此时导弧点端部距工件表面只有4 mm的距离，在焊接时离高温熔池很近，很容易发生烧损和污染。

3　电弧引燃过程的实际观测

为了对计算分析的结果进行验证，采用高速摄像技术对等离子—MIG 焊接枪体的起弧过程进行了拍摄。实际记录了等离子电弧借助 MIG 电弧起弧的路径和方式、等离子弧在平坦环电极上漂移的过程以及电弧在导弧点上引燃等过程，很好地验证了模拟计算分析的结果。

图 4 是所拍摄的平坦环形电极情况下的起弧过

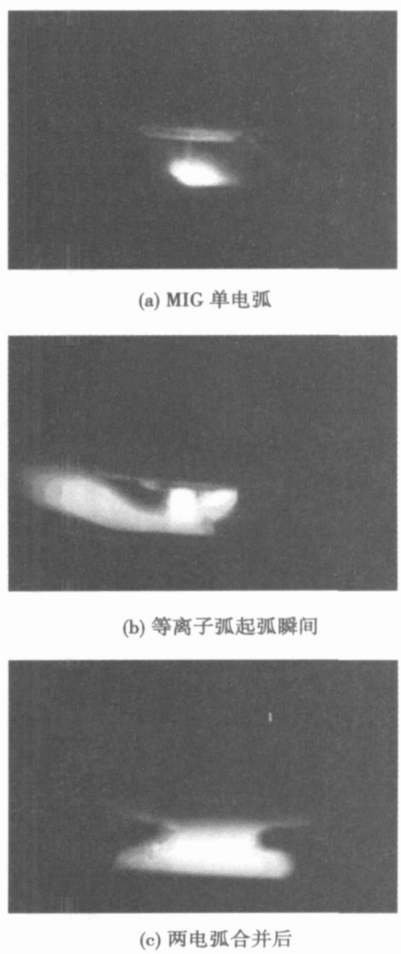

图 4　等离子—MIG 电弧的起弧过程

Fig. 4　Arc igniting of plasma — MIG welding

程。由图中可以明显看到等离子弧借助于 MIG 电弧提供的导电通道引燃的过程。其中图 4a 是仅有 MIG 电弧的情况。图 4b 中可以看到从喷嘴上产生了等离子电弧，然后与 MIG 电弧相接。最终两个电弧合并，并开始稳定燃烧(图 4c)。这种起弧的方式与前面计算的结果是完全符合的。

4 结 论

(1) 应用气体击穿理论分析了等离子—MIG 双电弧复合条件下的起弧过程，提出了用 Paschen 自变量 pd/T 判定等离子电弧起弧位置的方法。

(2) 通过模拟计算，分析了等离子电弧借助 MIG 电弧产生的导电通道起弧的过程。

(3) 利用模拟计算方法，探讨了利用导弧点分离等离子电弧和 MIG 电弧的可能性，并分析了导弧点长度对起弧路径的影响。

(4) 通过高速摄像方法实际拍摄了等离子—MIG 焊接的起弧过程，对计算结果进行了验证。

参考文献：

[1] Essers W G. Plasma with GMA welding[J]. Welding Journal, 1976, 5: 394—400.

[2] Schevers A A. Plasma-MIG welding of aluminium[J]. Welding and Metal Fabrication, 1976, 2: 17—20.

[3] Ton H. Physical properties of the plasma-MIG welding arc[J]. Journal of Physics D: Applied Physics, 1975, 8: 922—933.

[4] Essers W G, Jelmorini G, Tichelear G W. Arc characteristics and metal transfer with plasma-MIG welding[J]. Metal Construction, 1972, 4(12): 439—447.

[5] 侯清润，茅卫红，陈宜保. 气体放电实验与帕邢定律[J]. 物理实验，2004，24(1)：3—5.

[6] Petre A R, Bazavan M, Covlea V. Characterization of a DC plasma with hollow cathode effect[J]. Romanian Reports in Phisics, 2004, 56(2): 271—276.

[7] 文远芳. 高电压技术[M]. 武汉：华中科技大学出版社，2001.

作者简介：李德元，男，1959 年出生，博士，教授，博士研究生导师。主要从事焊接工艺与设备、表面强化技术方面的科研和教学工作。发表论文 70 余篇。

Email：dmy1962@sina.com

[上接第 88 页]

(3) 焊点中最大蠕变应变处节点的应变和应力随时间变化都显示出明显的周期性和积累效应。

参考文献：

[1] 郭 福，史耀武，夏志东，等. 无铅钎焊技术[M]. 北京：科学出版社，2006.

[2] Masazumi Amagai. Mechanical reliability in electronic packaging[J]. Microelectronics Reliability, 2002, 42: 607—627.

[3] Olaf Wittler, Hans Walter, Rainer Dudek, *et al*. Deformation and fatigue behaviour of AuSn interconnects[C] // Electronics Packaging Technology Conference, Shanghai, 2006: 297—301.

[4] 陈建钧，史 进，涂善东，等. BNi—2/0Cr18Ni9 钎焊接头高温蠕变行为的试验研究及数值模拟[J]. 焊接学报，2006，27(3)：39—43.

[5] 陈志刚. SnAgCuRE 钎焊接头蠕变行为的研究[D]. 北京：北京工业大学，2003.

[6] Schubert A, Dudek R, Auerswald E, *et al*. Fatigue life models for SnAgCu and SnPb solder joints evaluated by experiments and Simulation[C] // 53rd Electronic Components &Technology Conference, New Orleans, 2003, 603—610.

作者简介：韩永典，男，1983 年出生，博士研究生。主要从事无铅焊点可靠性方面的研究。发表论文 1 篇。

Email：hanyongdian@tju.edu.cn

welding was smaller than that of weld for MAG welding, and the strength of hybrid welded joint was higher than that of MAG welded joint, and hybrid welded joint rupture was ductile rupture.

Key words: low-power pulsed YAG laser; laser-arc hybrid welding; arc attraction and contraction; microstructure; ductile rupture

Effects of Ce on spreadability of Sn—Cu—Ni lead-free solder and mechanical properties of soldered joints SHI Yiping[1], XUE Songbai[1], WANG Jianxin[1], GU Liyong[2], GU Wenhua[2] (1. College of Materials Science and Technology, Nanjing University of Aeronautics and Astronautics, Nanjing 210016, China; 2. Changshu Huayin Filler Metals Co. Ltd., Changshu 215513, Jiangsu, China). p73—77

Abstract: Effects of rare earth Ce on spreadability of Sn—Cu—Ni solder on copper, mechanical properties of soldered joints and the microstructure of Sn—Cu—Ni—Ce solder were investigated respectively. The results indicate that with the increase of the content of Ce added to the Sn—Cu—Ni solder, the spreading area of Sn—Cu—Ni—Ce solder on copper was enlarged. When the content of Ce is about 0.05%, the spreading area is the largest and the microstructure of Sn—Cu—Ni solder is fine and uniform, and the mechanical properties of soldered joints are improved observably. Experimental results also show when the content of Ce is over 0.05%, the grains of the solder gradually become coarse, the spreadability of the solder descend, and the mechanical properties of soldered joints deteriorate as well.

Key words: Sn—Cu—Ni—Ce solder; lead-free solder; spreadability; mechanical properties; microstructure

Influence of ultrasonic peening treatment to gray cast iron welding cold crack YAN keng, NIE jie, YU huaidong, XU lv (Provincial key Lab of Advanced Welding Technology, Jiangsu University of Science and Technology, Zhenjiang 212003, Jiangsu, China). p78—80, 84

Abstract: To study the influence of ultrasonic peening treatment to welding cold crack, the tests were conducted on the specimens made of gray cast iron. Research focused on restraint stress and quenched structure of the three main reasons to induce the welding cold crack. Test method of cold crack was slit type cracking test. The test results show that by peening the whole weld on the one hand, the ultrasonic peening treatment can reduce the residual stress at the most degree. That is the residual stress R_1 are—53 and—57 MPa, R_2 are—37 and—80 MPa on the two specimens weld. On the other hand, the ultrasonic peening treatment can accelerate to form the nodular graphite cast iron and eliminate white cast iron, and the weld is made of nodular graphite cast iron after ultrasonic peening treatment. The reasonable ultrasonic peening treatment can absolutely avoid welding cold crack by reduce the residual stress and quenched structure.

Key words: ultrasonic implement treatment; residual stress; welding cold cracking

High-frequency pulse modulated variable polarity welding power and its arc pressure QIU Ling, FAN Chenglei, LIN Sanbao, YANG Chunli (State Key Laboratory of Advanced Welding Production Technology, Harbin Institute of Technology, Harbin 150001, China). p81—84

Abstract: A novel variable polarity welding power with high-frequency pulse modulation is designed by means of superimposed circuit, which can produce arc characteristics of high-frequency pulse welding in variable polarity welding process. Based on mathematic model of arc pressure and process experiment, the high-frequency pulsed current can increase arc pressure in a large scale. In the same root-mean-square welding current, the arc pressure with high-frequency (5 kHz) pulsed current increase to 2 times of the normal tungsten inert-gas welding arc, and it helpful for increasing of arc stiffness and energy density. It also provides theoretical proof for further researches on the high-frequency pulse modulated variable polarity welding.

Key words: variable polarity welding; high-frequency pulse current welding; arc characteristics; arc pressure

Numerical simulation of creep behavior of SnAgCu-CNT lap shear solder under thermal cycles HAN Yongdian[1], JING Hongyang[1], XU Lianyong[1], WEI Jun[2], WANG Zhongxing[3] (1. School of Materials Science and Engineering, Tianjin University, Tianjin 300072, China; 2. Singapore Institute of Manufacturing Technology, 71 Nanyang Drive 638075, Singapore; 3. Bulter (Tianjin). inc, Tianjin 300457, China). p85—88, 92

Abstract: Distribution of creep strain and stress of SnAgCu-CNT lap shear solder was studied under conditions of 125——40 ℃ by means of finite element method (FEM). The results show that obvious shearing deformation is found on the lap solder after 4 thermal cycles, then is the visible displacement on the upper and lower surfaces. Maximum equivalent creep strain lies in the middle of length orientation of solder-pad surfaces, while minimum strain lies in the center of solder. FEM results coincide well with experiment results. The curve of equivalent creep strain and stress versus time in the node of maximum equivalent creep strain exhibit apparent periodicity and build-up effect.

Key words: finite element method; SnAgCu-CNT; lap solder; equivalent creep strain

Igniting pattern of plasma-MIG welding Li Deyuan, Zhang Yishun, Dong Xiaoqiang (School of Materials Science and Engineering, Shenyang University of Technology, Shenyang 110023, China). p89—92

Abstract: In order to analyze the arc igniting course of the plasma-MIG (metal inert-gas) dual-arc welding, Paschen law was introduced to calculate the breakdown voltage on the different arc igniting paths. The effect of disruptive distance and temperature on the arc ignition was studied. The pattern that the plasma arc ignites by means of the breakdown path provided by the MIG arc was proved. It has been shown that the temperature and type of the shield gas must be taken into account when the lowest breakdown voltage on different igniting path was compared. Paschen law is suitable for analyzing the effect of these parameters, and can be used to predict the igniting path of the second arc. The method can also be used to other

dual-arc welding method. Finally, the actual arc igniting course was observed and analyzed by high speed video camera.

Key words: welding; plasma arc; metal inert-gas arc; arc igniting; Paschen law

Mechanical properties and microstructure of X70 butt joint welded by self-shielded flux cord wire PAN Chuan[1], YU Ping[1], TIAN Zhilin[1], XUE Zhenkui[2] (1. China Iron & Steel Research Institute Group, Beijing 100081, China; 2. Pipeline Research Institute of CNPC, Langfang 065000, Hebei, China). p93—96

Abstract: The present paper deals with the research work of self shielded flux cored wire (FCAW-S) for X70 large diameter pipe. Welding procedure qualifications tests and mechanical properties tests were carried out by Pipeline Research Institute of CNPC to assess field weldability and should be in accordance with API 1104 and the additional standard requirements. The results of welding procedure qualifications tests show that the self-made FCAW-S has good all-positions weldability, detachability, arc stability and less spatter loss coefficient and total amount of weld fumes. The tensile strength of the weld is about 730—760 MPa and the average impact absorbing energy at —20 ℃ is 125 J. Tests results show that this self-made FCAW-S can provide a qualified weld for X70 pipeline steel. The microstructure of X70 butt joint weld exhibits acicular ferrite, polygonal ferrite, proeutectoid ferrite, bainite morphology but shows no weidmanstaten structure in HAZ (heat-affected zone) coarse grain zone. The main microstructure in columnar crystal zone and HAZ coarse grain zone is bainite. Bainitic microstructure in the butt joint indicated this self-made FCAW-S have the capability to meet all mechanical properties requirements of this welding material.

Key words: X70 Pipeline steel; self-shielded flux cored wire; properties; microstructure

Welding technology and microstructure and properties of welded joint of high strength and hardness alloy steel for tandem GMAW FENG Yuehai, WANG Kehong, WANG Jianping, GU Minle (Department of Materials Science & Engineering, Nanjing University of Science and Technology, Nanjing 210094, China). p97—100

Abstract: Tandem GMAW (gas metal arc welding) is high efficiency welding technology for high strength and hardness alloy steel in heavy vehicles was studied. Austenitic stainless steel wire was adopted to make welding process experiment for high strength and hardness alloy steel, and the performance and microstructure of the joint were researched. The experiment results proved the good joint of high strength and hardness alloy steel was attained with tandem GMAW.

Key words: tandem; welding parameters; joint properties; microstructure

Engineering estimation method of 5A06 aluminum alloy's material properties by PDS ZENG Zhi, WANG Lijun (School of Materials Science and Engineering, Tianjin University, Tianjin 300072, China). p101—104

Abstract: The 5A06 aluminum alloy is one kind of basic welding materials, but its thermo physical parameters, especially at the high temperature, have been hardly determined under the general project condition, which have great influence on the accuracy of engineering computation. The best annealing temperature of 5A06 Al alloy was confirmed with engineering experiment, based on the rebound after annealing, and the finite element model was built, and the thermo physical parameters were estimated with the probability design system (PDS) in the finite element software ANSYS. The analysis indicated that, the obtained material attribute values accord with the project reality. The use of the probability design system provides one of the phenomenological effective methods for the solution of the unknown material attributes.

Key words: 5A06 aluminum alloy; probability design system; material properties; annealing

Stress-strain cycles of titanium alloy welding process LI Ju[1], GUAN Qiao[1], SHI Yaowu[2], GUO Delun[1] (1. Beijing Aeronautical Manufacturing Technology Research Institute, Beijing 100024, China; 2. School of Material Science and Engineering, Beijing University of Technology, Beijing 100022, China). p105—107

Abstract: The welding thermal elasto-plastic stress-strain cycles diagram (shortly WSS diagram) describes the welding stress-strain relation on the whole. The stress-strain cycle in every area is the necessary part of the WSS diagram. The stress and strain relations of the points with different distances from the weld centerline on the specimen were investigated. The states of stress and strain of some point on the specimen during the welding process could be derived. On the basis of these results, the stress and strain relation in the each area of WSS diagram can be derived, and the diagram is described quantitatively, which make it easy to understand the WSS diagram. The results showed that the longitudinal stress-strain cycles are different in the different areas in the diagram. During the cooling process, weld and the zone nearby are in the unloaded states.

Key words: titanium alloy; welding; stress; strain

Review and prognosis of state of arts on force sensing and control for robotic remote welding WEI Xiuquan, LI Haichao, GAO Hongming, WU Lin (State Key Laboratory of Advanced Welding Production Technology, Harbin Institute of Technology, Harbin 150001, China). p108—112

Abstract: Force sensing and force control are crucial for the successful execution of contact manipulation in unstructured environment for robotic remote welding. In this paper, reaserch on the theory of robot force control and the strategy of embedding force control into industrial robots are reviewed. Focusing on the fundamental issues in contact task, appropriate force control strategies for remote welding are presenteded. The using of force sensing and control technology in some aspects of robotic remote welding field, such as bilateral force-feedback teleoperation, contact force control and force-based pricise task environment modeling, are emphasized. At last, some research topics and investigation trends are proposed.

Key words: force sensing; force control; robotic remote welding